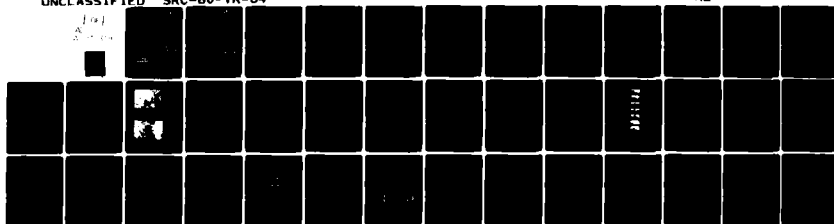
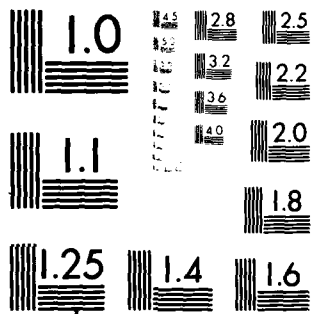


AD-A097 109

SHAKER RESEARCH CORP BALLSTON LAKE N Y F/G 13/9
LABORATORY INVESTIGATION OF WATER-LUBRICATED ELASTOMERIC BEARING--ETC(U)
JAN 81 R L SMITH, A I KRAUTER, C H PAN N00014-74-C-0278
UNCLASSIFIED SRC-80-TR-64 NL



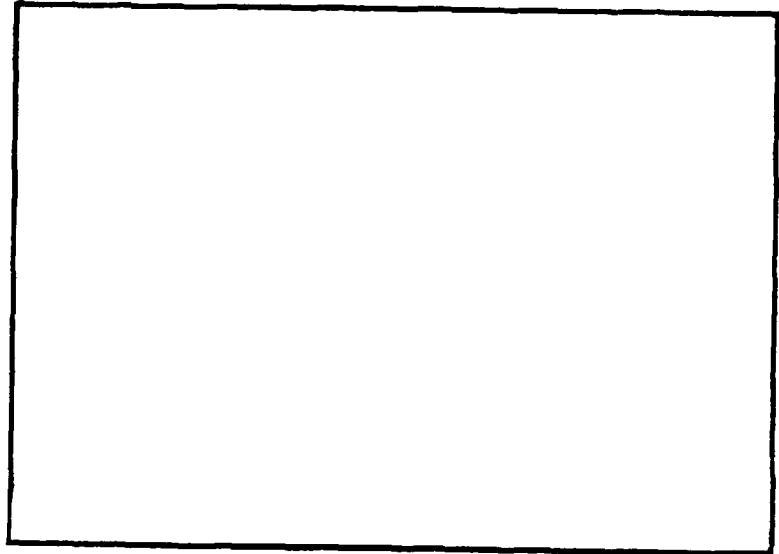
END
DATE
FILMED
8-8
DTIC



MICROCOPY RESOLUTION TEST CHART
NATIONAL BUREAU OF STANDARDS 1963-A

(12) LEVEL II

AD A 097109



DTIC
ELECTE
MAR 3 1 1981
S B

SHAKER

Research Corporation

DISTRIBUTION STATEMENT A

Approved for public release;
Distribution Unlimited

81 3 13 019

(12) LEVEL II

TECHNICAL REPORT

SRC 80-TR-64

LABORATORY INVESTIGATION OF
WATER-LUBRICATED
ELASTOMERIC BEARINGS

Prepared under

Contract No. N00014-74-C-0278

Prepared for

Office of Naval Research
Arlington, Virginia

DTIC
ELECTE
S MAR 31 1981 D
B

January, 1981

Prepared by

R. L. Smith
A. I. Krauter
C. H. T. Pan

DISTRIBUTION STATEMENT A

Approved for public release;
Distribution Unlimited

SHAKER RESEARCH CORPORATION
Northway 10 Executive Park
Ballston Lake, N. Y. 12019

UNCLASSIFIED

SECURITY CLASSIFICATION OF THIS PAGE (When Data Entered)

REPORT DOCUMENTATION PAGE		READ INSTRUCTIONS BEFORE COMPLETING FORM
1. REPORT NUMBER	2. GOVT ACCESSION NO.	3. RECIPIENT'S CATALOG NUMBER
	AD-A097109	
4. TITLE (and Subtitle)	5. TYPE OF REPORT & PERIOD COVERED	
Laboratory Investigation of Water-Lubricated Elastomeric Bearings.	Research and Development Technical Report	
6. AUTHOR(s)	7. PERFORMING ORG. REPORT NUMBER	
R. L./Smith A. I./Krauter C. H. T./Pan	SKC-80-TR-64	
8. PERFORMING ORG. NAME AND ADDRESS	9. CONTRACT OR GRANT NUMBER(s)	
Shaker Research Corporation Northway 10 Executive Park Ballston Lake, N. Y. 12019	N00014-74-C-0278	
10. CONTROLLING OFFICE NAME AND ADDRESS	11. PROGRAM ELEMENT, PROJECT, TASK AREA & WORK UNIT NUMBERS	
Office of Naval Research Arlington, Virginia 22217		
12. MONITORING AGENCY NAME & ADDRESS (if different from Controlling Office)	13. REPORT DATE	
Naval Sea Systems Command Code 5243 Washington, D. C. 20362	January 1981	
	14. NUMBER OF PAGES	
	31	
	15. SECURITY CLASS. (of this report)	
	UNCLASSIFIED	
	16. DECLASSIFICATION DOWNGRADING SCHEDULE	
17. DISTRIBUTION STATEMENT (of this Report)		
<div style="border: 1px solid black; padding: 5px; text-align: center;"> DISTRIBUTION STATEMENT A Approved for public release; Distribution Unlimited </div>		
18. DISTRIBUTION STATEMENT (of the abstract entered in Block 20, if different from Report)		
19. SUPPLEMENTARY NOTES		
20. KEY WORDS (Continue on reverse side if necessary and identify by block number)		
compliant layer bearings vibration squeal stern tube noise stability water lubrication stick slip friction rubber bearing		
21. ABSTRACT (Continue on reverse side if necessary and identify by block number)		
This report concerns an experimental laboratory study of the sliding friction behavior of water-lubricated rubber stave bearings. Speed-dependent friction characteristics were measured because they are associated with the phenomenon of audible self-excited vibrations. As part of an effort to establish guidance for the design of noise-free stern tube bearings, the friction-speed curves for five modified de-		

DD FORM 1473 1 JAN 73

EDITION OF 1 NOV 65 IS OBSOLETE
GPO 0-102-114-0001

UNCLASSIFIED

SECURITY CLASSIFICATION OF THIS PAGE (When Data Entered)

UNCLASSIFIED

SECURITY CLASSIFICATION OF THIS PAGE (When Data Entered)

signs were obtained and were compared with those for a conventional design.

The reference conventional stave bearing used in this study is similar in cross-sectional design to that used aboard ship for propulsion shaft support. The modified designs were produced from the conventional design by inserting brass cylinders into the stave near the rubber-stave backing interface. The "swing pad" stave, which features several laminated brass layers and a conformal load bearing surface, was also included in the study. Testing conditions included a speed range of 0 to 1.36 m/s and a unit normal load range of 105 to 689 kPa.

The results obtained show that changes in the friction-speed curve were produced by the stave modifications. Since the friction speed curve is one of the contributors to bearing vibrations, stave design modifications have the potential for avoiding such vibrations.

SECURITY CLASSIFICATION OF THIS PAGE (When Data Entered)

TABLE OF CONTENTS

	<u>Page</u>
1.0 INTRODUCTION _____	1
2.0 BACKGROUND AND APPROACH _____	4
3.0 DISCUSSION OF EXPERIMENT _____	7
3.1 Description of Test Apparatus _____	7
3.1.1 Mechanical Design Modifications _____	7
3.1.2 Instrumentation _____	12
3.1.3 Test Staves _____	15
3.2 Description of Tests _____	18
3.3 Results for Friction vs. Speed with Load Effects _____	20
4.0 SUMMARY AND CONCLUSIONS _____	28
5.0 RECOMMENDATIONS _____	30
6.0 REFERENCES _____	31

Accession For	
NTIS GRA&I	<input checked="" type="checkbox"/>
DTIC TAB	<input type="checkbox"/>
Unannounced	<input type="checkbox"/>
Justification	
PER LETTER	
By _____	
Distribution/ _____	
Availability Codes	
Dist	Avail and/or Special
A	

LIST OF FIGURES

<u>Figure Number</u>		<u>Page</u>
1.1	Typical Friction Versus Sliding Speed for Single Test Load _____	2
3.1	Closeup of Stave Support Structure _____	8
3.2	Top View of Experimental Apparatus _____	8
3.3	Drive Train Diagram Showing Relative Positions of Some Test Rig Components and Features _____	10
3.4	Test Instrumentation Block Diagram Showing Friction and Speed Measurement Technique _____	13
3.5	Photograph of Test Stave Design Cross Sections _____	16
3.6	Friction-Speed Curves for Six Different Test Bearing Loads _____	21
3.7	Friction Forces Versus Sliding Speed for Full Range of Test Loads and Stave Design Cross Sections _____	23
3.8	Friction Forces Versus Normal Loading for Full Range of Test Speeds and Stave Design Cross Sections _____	24
3.9	Swing Pad Friction Levels for Like "New" and "Worn" Stave Element that had been put through an Accelerated Wear Process _____	27

LIST OF TABLES

<u>Table Number</u>		<u>Page</u>
3-1	Operating Test Conditions _____	19
3-2	Sliding Friction Force Variations _____	26

ABSTRACT

This report concerns an experimental laboratory study of the sliding friction behavior of water-lubricated rubber stave bearings. Speed-dependent friction characteristics were measured because they are associated with the phenomenon of audible self-excited vibrations. As part of an effort to establish guidance for the design of noise-free stern tube bearings, the friction-speed curves for five modified designs were obtained and were compared with those for a conventional design.

The reference conventional stave bearing used in this study is similar in cross-sectional design to that used aboard ship for propulsion shaft support. The modified designs were produced from the conventional design by inserting brass cylinders into the stave near the rubber-stave backing interface. The "swing pad" stave, which features several laminated brass layers and a conformal load bearing surface, was also included in the study. Testing conditions included a speed range of 0 to 1.36 m/s and a unit normal load range of 105 to 689 kPa.

The results obtained show that changes in the friction-speed curve were produced by the stave modifications. Since the friction speed curve is one of the contributors to bearing vibrations, stave design modifications have the potential for avoiding such vibrations.

ACKNOWLEDGMENTS

The authors wish to acknowledge the efforts of Mr. S. A. Montross and Dr. D. D. Fuller for their contributions to the work described here. Mr. Montross gathered all the experimental data and Dr. Fuller made suggestions on how the rubber cross section could be changed for the investigative laboratory work.

1.0 INTRODUCTION

Ship propulsion shafting is commonly supported by water-lubricated bearings. The outboard shaft support bearings are designated as stern tube and strut bearings. Each of these bearing support structures is composed of several load carrying elements called staves. Staff element designs commonly used have been reported in References 1 - 4.

Each staff element consists of a long brass strip which has a synthetic rubber bonded to its load supporting surface. This rubber surface when flooded with sea water becomes the propulsion shaft sliding support bearing. Basically today's designs have good loading capacity and wear well. However, under certain operating conditions these bearings can cause and/or sustain a certain amount of vibration. Reported as having a "squeal" or "chatter" quality, these vibrations occasionally have rather large amplitudes and span a wide range of vibrational frequencies, including the audible.

Since the staff bearings are designed to operate with a unit loading of 280-310 kPa (40-45 psi) and spend much of their operating life at low sliding speed, these bearings frequently run in the boundary lubrication regime. Thus, the majority of the load is often carried through intimate contact between the rubber and the material of shaft construction. Most lubricating films generated during operation may be as low as 0.0254 to 0.508 μm (1 to 20 micro-inches) in thickness. Static and sliding coefficients of friction have been observed over the full range from essentially 0 to 1.0. In general, break-away friction is from 0.4 to 0.8 and decreases toward a lower level as operating speed increases. Fig. 1.1 is a typical curve of the observable friction coefficient for a water-lubricated staff bearing. The actual running friction of a staff has been observed to depend upon several variables including the

- surface conditions of the metal shaft
- wear history of the supporting rubber surface
- water condition, temperature, mineral content, etc.
- applied load
- running speed
- relative contact surface curvature

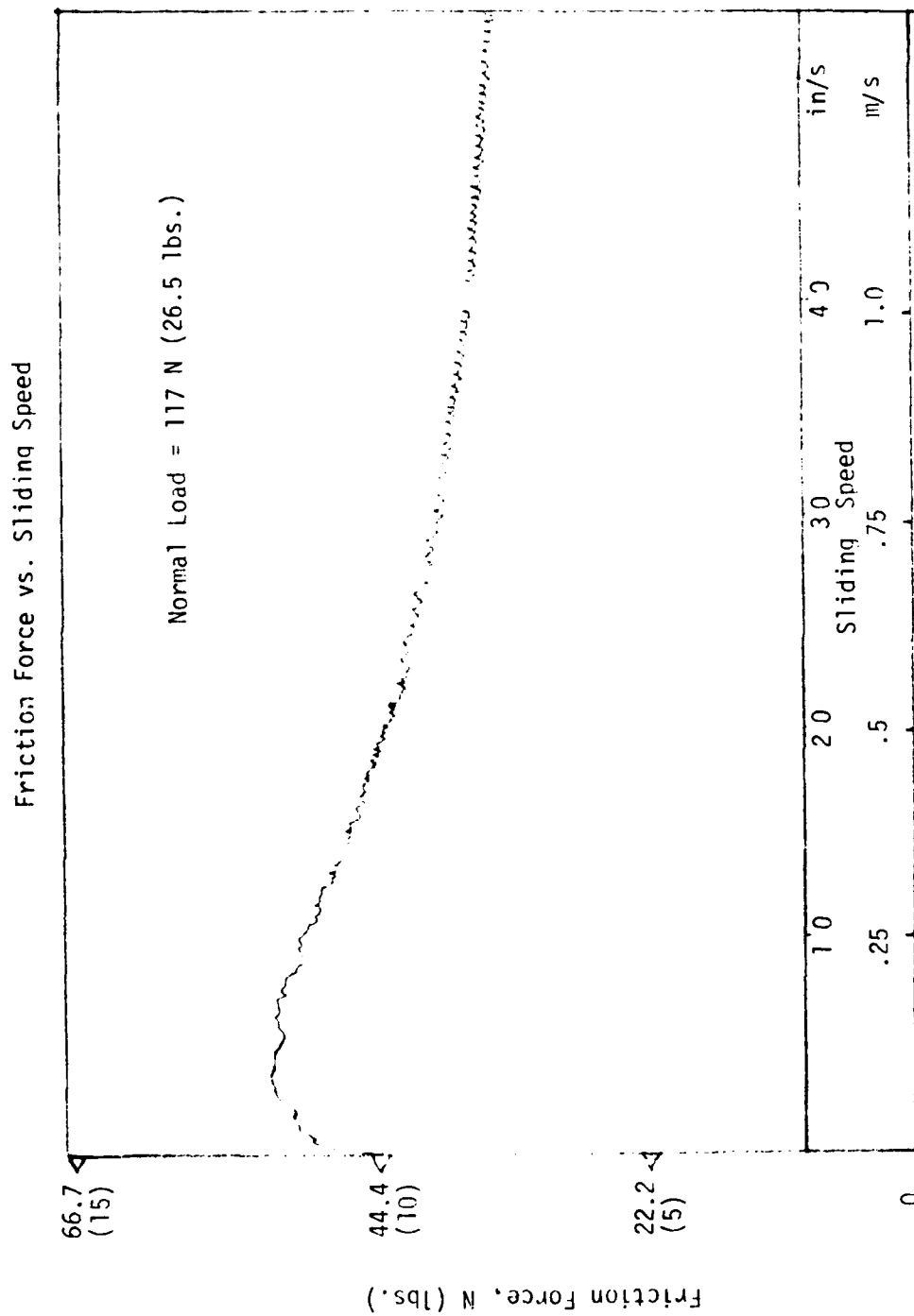


Figure 1.1 Typical Friction Versus Sliding Speed for Single Test Load

The negative slope characteristic of the friction-speed curve dominates the cause-effect relation of the "squeal" or "chatter" which would not occur if the friction-speed curve were positively sloped.

It is the purpose of this report to investigate the influence of the stave design on the frictional speed characteristics of the bearings. To do this, several modified stave designs were tested in a laboratory, water-lubricated rig. The majority of the modified designs contain embedded brass elements within the rubber portion of the stave itself. These stiffening inserts were intended to modify the lubrication performance of the sliding surface by changing its compliance characteristics. Included in the tests was the "swing pad" design which is constructed of multilayers of brass and rubber. In addition, this design has a contoured upper surface which nearly conforms to the shaft it is intended to support.

2.0 BACKGROUND AND APPROACH

Stern tube bearings have been subjected to laboratory tests (References 1 - 6) for many years. In a past study (4) specific stave bearing factors such as mounting compliance, structural damping, and the slope of the friction-speed curve were identified as important parameters in the operation of the bearings. Previous studies had produced a working test rig, instrumentation capabilities, experimental techniques, and analytical procedures for evaluation of test bearing data. In this section some aspects of the previous work will be presented. In addition, the technical approach of the present study is discussed in some detail.

Rubber bearings have been known to be prone to vibratory behavior under some conditions of operation. Laboratory production of the type of vibration experienced in the field was the primary objective of one of the earlier studies (6). Rubber bearing noise was produced in those early tests by loading a stave element against a transparent disk. Actual sounds and spectra of their emission were examined and photos of the emitting interfaces were taken. Control of the vibratory emission was not established and no mechanism of noise generation was determined.

Following that study an experimental apparatus was designed and constructed (5). The test apparatus was used for the examination under laboratory conditions of small sections of rubber bearing staves. The test device was capable of quiet and smooth operation and provided a system for controlled examination of stave elements.

In subsequent laboratory work (2) the test bed was used to demonstrate the ability of producing controlled quantifiable noise. The work resulted in a qualitative description of the squeal phenomenon. It was suggested that squeal/chatter was the consequence of an unstable vibrational mode. In the experimental apparatus used, one such mode corresponded to the motion of the test stave in a circumferential direction with respect to the disk. It was also suggested that production of audible noise need not be associated with instantaneous disappearance of rubber/disk relative motion (i.e.,

"stick" need not occur). From these qualitative descriptions of the squeal/chatter phenomenon, both a simple analytical model and an improved pad mounting design for the experimental apparatus were produced (4).

In (4) the analytical model and the improved pad mounting design were used to quantify squeal/chatter vibrations. The technical approach taken employed the analytical model to predict the onset of squeal/chatter in the experimental apparatus. Success in this prediction of squeal/chatter tendency led to the following conclusions:

- o the squeal/chatter mechanism was explained for the experimental apparatus,
- o the squeal/chatter mechanism can, in principle, be quantified,
- o squeal/chatter results from the growth of an unstable vibration mode,
- o the structural damping and slope of the friction-speed curve are important factors in the generation of the squeal/chatter vibration.

This previous work (4) suggested that one way to eliminate squeal/chatter is to modify the slope of the friction-speed curve. The present report is concerned with the possibilities of effecting such a modification through changes in stave design. Several changes in stave design can be envisioned. Perhaps the simplest is to change the compliance characteristics of the stave in a manner that encourages the formation of a water film at the stave/shaft interface. A change which may do this is one that produces a normal compliance decrease with distance from the leading edge.* Such

* In a conventional stave, the rubber material is thickest at the center of the cross-section. This leads to low compliance at the leading edge and high compliance at the center of the cross-section of the stave.

a change in the conventional stave therefore was made and the resulting changes in the friction speed curve were measured.

Because of recent success in shipboard use of swing pad staves, one such stave was also included in the present effort.

To obtain the friction-speed curves for the tested staves, the following detailed work was performed. This work consisted of

1. Minor rig modifications, including:
 - a. higher unit normal load capability;
 - b. alternate load and speed measurement techniques above and beyond those employed in the past;
 - c. mechanical drive stiffening and test disk support modifications for the expected higher loading levels.
2. Preparation of the modified stave bearing elements.
3. Experimental testing of the bearing stave elements prepared.

The description of the test rig and its modifications is contained in Section 3.1.1. The newly provided instrumentation is discussed in Section 3.1.2. Stave modification and cross-sectional designs are presented detailed in Section 3.1.3.

The overall test results and data are given in Section 3.2, and Section 4.0 is composed of the summary of these examinations.

3.0 DISCUSSION OF EXPERIMENT

This section presents overall design features of the test rig and discusses recent modifications made in preparation of subsequent testing of the compliant rubber stave bearings. Also included is a discussion of the types of tests performed and the resulting test information gathered.

3.1 Description of Test Apparatus

The test apparatus used in gathering friction-speed data from a short single element stave bearing section is shown in Figs. 3.1 and 3.2. The assembly shown in the photo has been previously discussed in References (2), (4) and (5) and was modified in several ways for the present test work. Test rig modifications and overhaul included

- a new friction (tangential) force measurement technique
- replacement of the drive shaft of the test rig
- increased loading capacity on the sliding test bearing
- an improvement in the shaft (rotational) speed readout
- water line filtering for control of contaminants, and
- addition of high capacity supports in the rig.

3.1.1 Mechanical Design Modifications

Friction Force Measurement

Recent test rig alterations provided for a new friction (tangential) force measuring concept on the mounted test pads. The past work had been conducted with a piezoelectric force cell as shown in Fig. 3.2. The time constant of the piezoelectric force cell is relatively short and was previously used in a relatively rapid run-down mode. A capability for steady state measurement of friction was needed for slow speed runs and was achieved by adding a precision displacement sensor to the test rig (position shown in Fig. 3.2). This sensor was calibrated for tangential reaction loads applied to the stave mounting block depicted in Fig. 3.1.



Figure 3.1 Diagram of Stave Support Structure

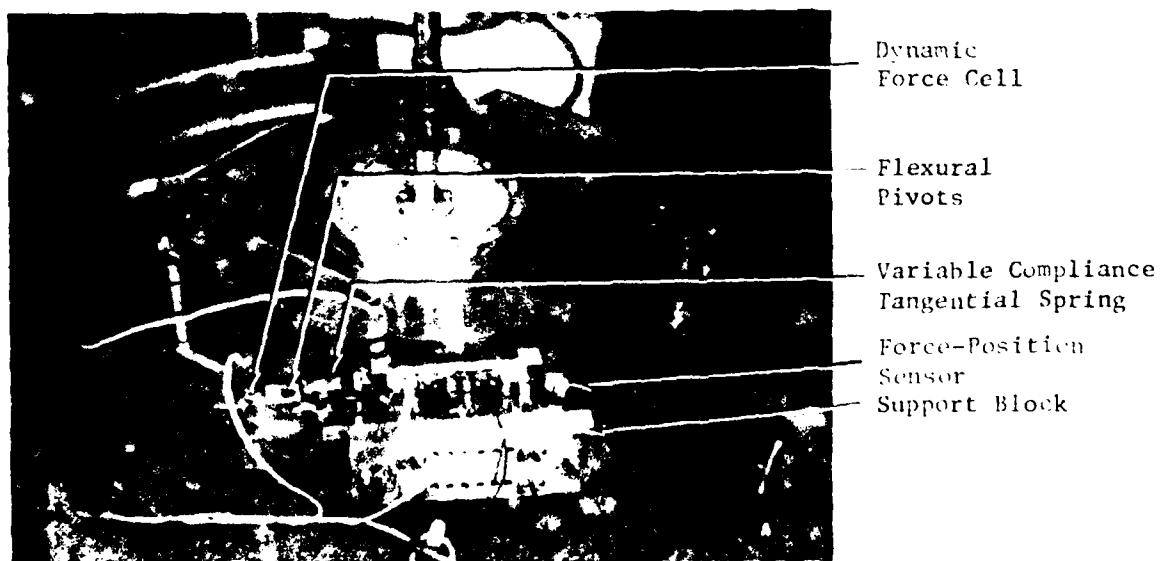


Figure 3.2 Detail of Experimental Apparatus

Calibration consisted of applying known tangential loads to the stave mounting block and noting the reaction directly on the x-y plotter used for friction-speed output measurement. Calibration of the friction reactive force was performed with no load on the test stave itself. Calibration loading was applied in the same direction as that of the expected frictional force applied by the disk to the stave. In addition, the test stave when loaded normally without the rig test shaft rotating indicated no tangential frictional force output.

Drive Shaft Stiffening

The present test work was performed with a much stiffer drive axle than used in the past. The steel woven flexible drive axle was replaced with a solid steel axle with universal joints as shown in Fig. 3.3. The universals and the drive shaft were coupled with locked keys. The universal joints were machined for a minimum of clearance around the connecting axle shafting to prevent the possibility of having torsional dead band and/or backlash between the drive motor and the test rig disk. A relatively rigid torsional connection was obtained. The universal joints were effective in avoiding inadvertent lateral loading due to misalignment.

Increased Loading Capacity

Stave loading in the present rig is derived from a hydrostatic water-actuated bearing and piston. This piston loader is positioned directly across the rotating disk from the test rubber stave. The supply pressure to the hydrostatic bearing on the face of the load piston and on the cylindrical sides of the load piston has been significantly increased. This pressure supply increase widens the loading range of the test rig by insuring that the loading piston does not come into

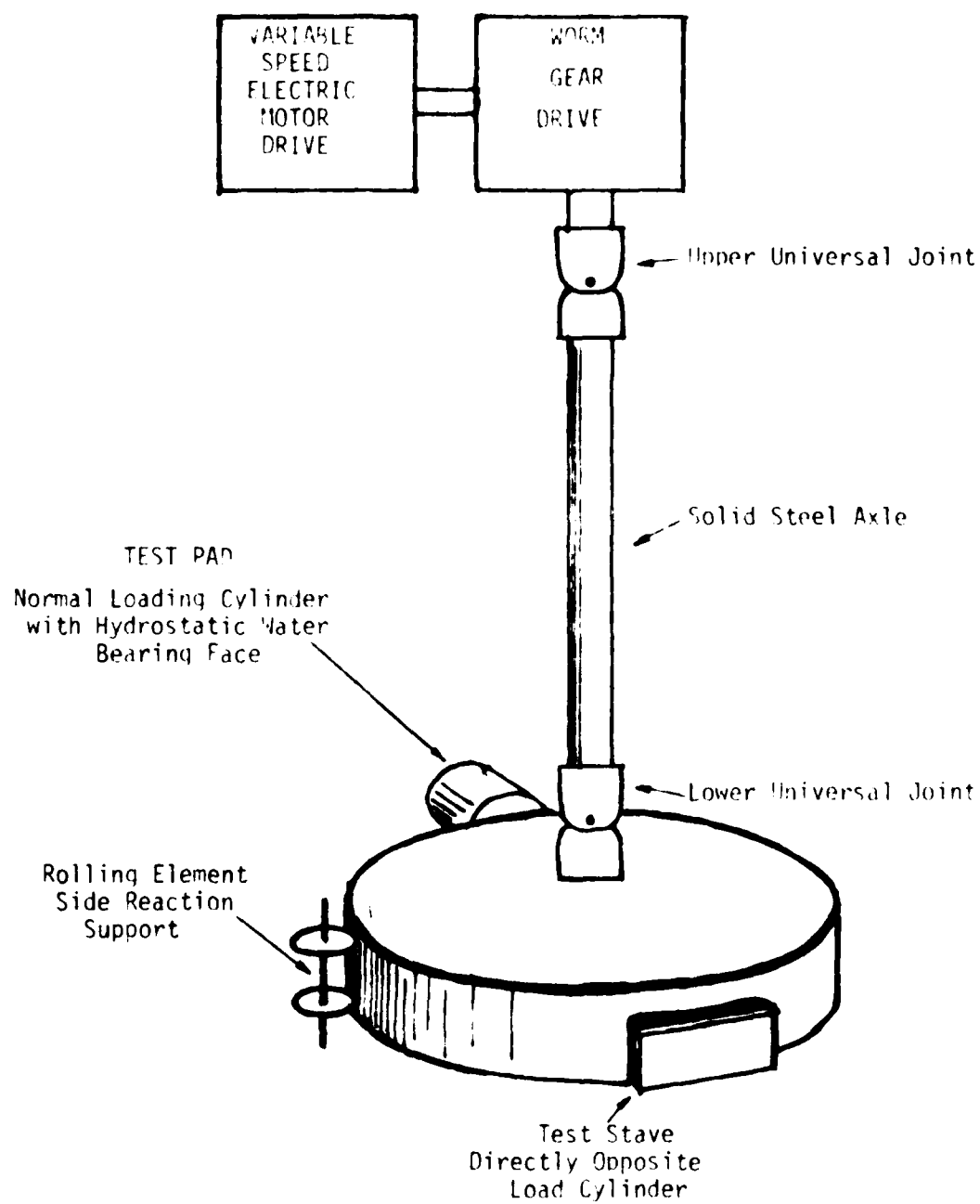


Figure 3.3 Drive Train Diagram Showing Relative Positions of some Test Rig Components and Features.

contact with the test rig rotating disk. Applied test pad loads of 4 to 5 times those possible in the past are now available.

Test Shaft Rotational Speed

Past performance testing incorporated a shaft encoder and frequency-to-direct current ratio for measurement of speed. This made precise recording of sliding speeds in the 0 to 0.079 m/s range difficult to obtain. The present work incorporated a direct current generating source which gave a D.C. voltage proportional to shaft speed over the full operating range from 0 to 1.2 m/s. Test shaft speed calibration was set up on the x-y plotter through visually clocking the shaft rotational frequency with a stop watch through a one-to-two minute timing cycle.

Water Line Filtering

The rotating test disk weight is supported by hydrostatic water bearings. In the past it has been found that both these support bearings and the loading piston has required cleaning. Particulate contaminants in the water supply and debris generated by rubbing of pump rotor on occasion plugged the feeding ports and degraded their operation. In order to eliminate this problem in the present work, in-line filters were installed. The filter worked very well and at no time did the hydrostatic bearings need to be cleaned after the filters were installed.

Side Reaction Loads and Support Elements

With increased capacity of the loading piston, correspondingly higher capability in the side load supports became necessary. Originally the side loads were supported by hydrostatic pads. Although higher hydrostatic load capacity could be realized by using higher pressure, it was decided to replace the hydrostatic side supports with a pair of identical rolling element devices as illustrated in Fig. 3.3 which are less likely to react with excessive friction in an overload condition.

3.1.2 Instrumentation

The essential features of the test rig instrumentation are shown in block diagram form in Fig. 3.4. The basic instrument elements of this test set-up consisted, in addition to the rig drive and disk support structure, of

- o a pressure gage for detecting and setting the applied normal loads placed on the test bearing stave,
- o a direct current generating rotational speed sensor,
- o a tangential stave bearing force sensor, and
- o an x-y plotter for visually displaying and recording the test results.

Normal Loading of Stave

An in-line pressure gage was used as an indicator to set and measure the amount of load being applied across the test disk, and hence, on the test stave bearing.

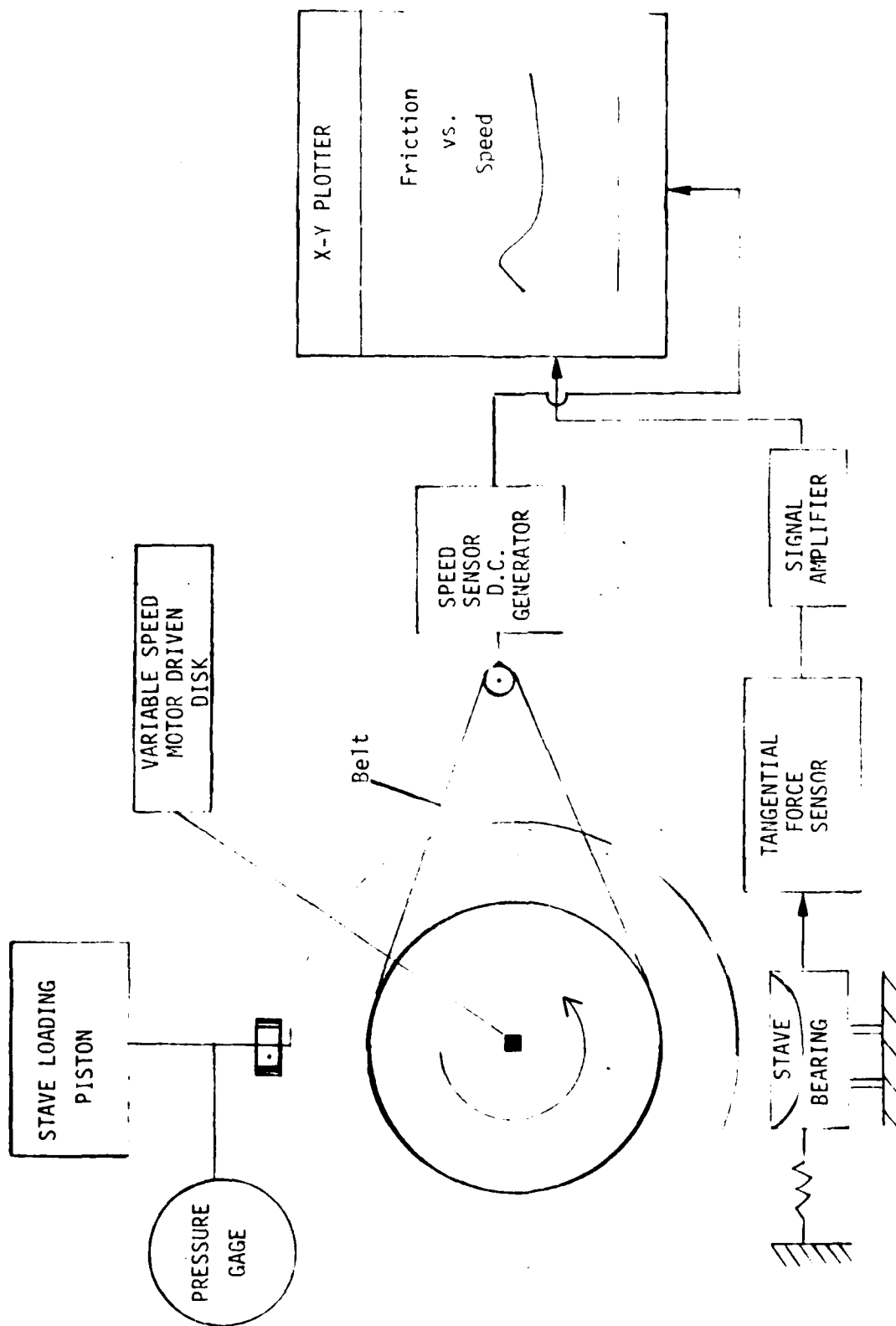


Figure 3.4 Test Instrumentation Block Diagram showing Friction and Speed Measurement Technique

All tests staves are nominally .025 m (1.0 in) long and .070 m (2.75 in) wide, so that nominal unit loads based on the projected area varied from 22 kPa to 152 kPa (3.2 psi to 22.0 psi). "True contact area" during testing was much smaller and could be estimated by inspection of the surface wear pattern; accordingly "true unit load" was estimated to range from 105 kPa to over 689 kPa (15 psi to over 100 psi).

Speeds used in testing were set and varied by hand with the aid of the operator control knob on the motor speed controller.

Disk Rotational Speeds

Visual tracking of test disk rotational speed was performed by observing the X-Y plotter pen position on prescaled plotter paper. Scaled axes in meters per sec were determined by clocking shaft rotational frequencies with a stopwatch. Accuracy of speed measurement was within $\pm 2\%$ in the high range of speeds from 0.32 m/s to 1.36 m/s. Speed measurement accuracy below 0.32 m/s approached a fixed value of about ± 0.016 m/s as a result of plotter scaling technique.

The output signal from the tachometer generator was very clean and stable and required no filtering or amplification in order to drive the plotter.

Stave Friction Force Detection

Stave bearing friction forces were determined by sensing the small translational motion of the stave mounting block. This motion in most of the tests amounted to less than 0.05 mm (0.002 inch) of total translation. An accurate displacement probe D.C. signal was amplified and used to drive the recording X-Y plotter during each test condition of loading. Calibrations of

stave mounting block translational position and load were determined by applying various known amounts of force to the stave mounting. The displacement (resulting force) signal was fully amplified and run to the plotter during calibration and then all electronic settings were left fixed during that portion of the testing.

Calibration of loading revealed this sensing technique to be linear over the majority of test range loads. However, some stiffening of the support structure was noted at high loads, which rendered the scale non-linear.

Since these loads were outside the majority of those used in testing, it did not hamper data gathering. For those tests where the friction calibration was in the non-linear range a point-by-point transfer of the scale was performed for evaluation purposes.

Recording Results on X-Y Plotter

The signals of speed and friction measurement were fed to a standard X-Y plotter with vernier offset and electronic scale adjustment capability, providing "instant" display of the friction versus speed test results. Direct recording in this manner also allowed visual checking of sensor-to-recorder calibration signals of rig test parameters.

3.1.3 Test Staves

Several test staves were used in the work presented in this discussion. A total of six different pad geometries were considered by the laboratory test rig. Variations in stave designs tested are shown in the photograph of Fig. 3.5.

A previously published report (Ref. 4) discussed the desirability of modifying the friction-speed curve to control or to minimize squeal/chatter vibrations. The stave sections in Fig. 3.5 were developed in order to assess the potential of altering this curve. The

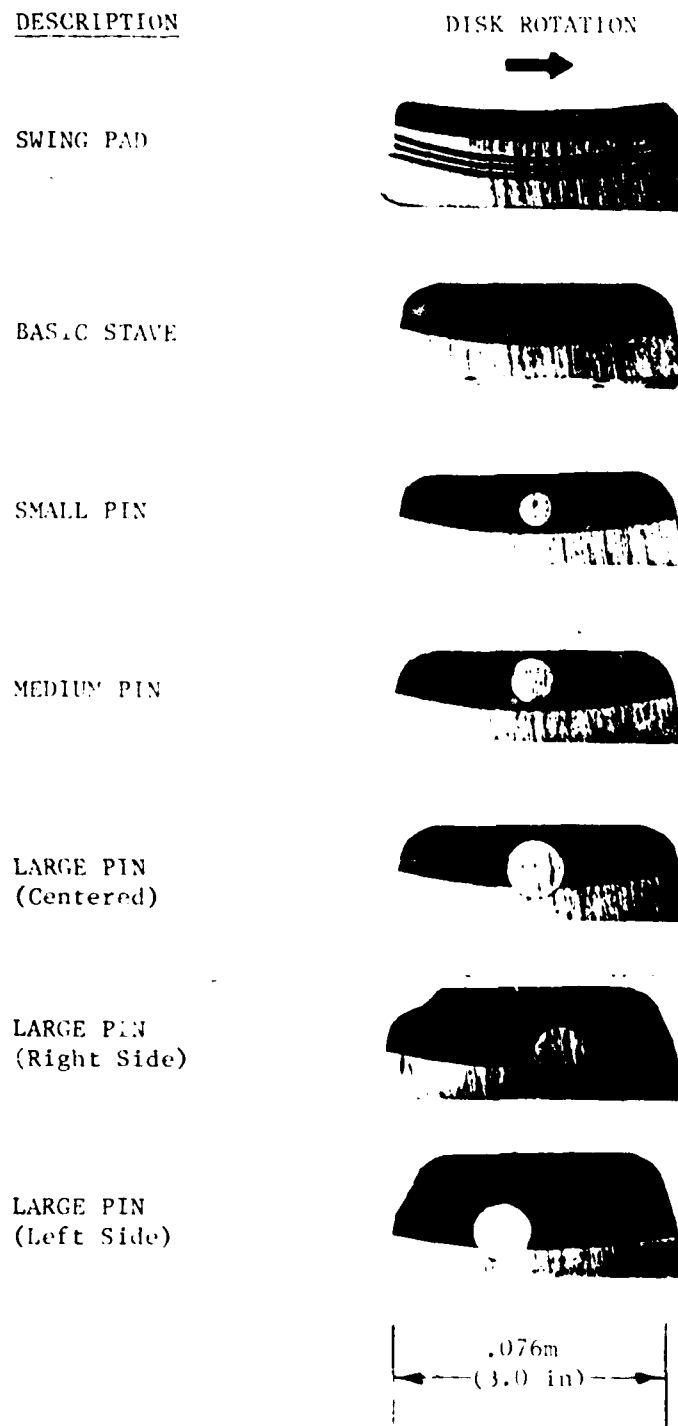


Figure 3.5 Photograph of Test Stave Design Cross Sections

intent of adding the pin to the stave was to modify its compliance characteristics so that the maximum compliance is at the edges of the cross-section and the minimum compliance is at the center of the cross-section. With this compliance distribution, there is an increased likelihood (compared to that for the basic stave) of forming a hydrodynamic water film at low shaft speeds. With such a water-film, the variations in friction-speed slope might be reduced, thereby reducing the magnitude of the low speed negative slope of the curve. This, in turn, would tend to reduce squeal/chatter as indicated in (4).

The non-standard cross-sectional test stave designs shown in Fig. 3.5 were obtained by drilling axial holes in the stave and by then inserting brass pins. The brass pins were slightly larger than the holes, so that several pounds of force were needed to insert each pin into its hole. All stave test sections, except the swing pad test stave, were obtained by cutting the test sections from the same bearing stave.

The cylindrical pins used ran the full length of the test pad and were 0.0095, 0.012, 0.0158 m (0.375, 0.500, and 0.625 inches) in diameter. Three pads were constructed with the pin inserted concentrically along the normal axis of the stave length. Several pads with the 0.0158 m (0.625 inch) diameter pins were tested. One pad had the pin centered, whereas in the others it was offset from the bearing load supporting contact line (see lower two designs shown in Fig. 3.5). Depending upon the relative running direction of the shaft on this pad, it was anticipated that different lubricating films would be generated during operation; and thus different amounts of friction.

Slight differences of the stiffening pin placement within the rubber itself existed between the large 0.0158 m (0.625 inch) diameter and the other two staves with smaller pins. The larger 0.0158 m (0.625 inch) diameter was mounted in intimate contact with the backing of the stave bearing brass whereas the two small pins were placed within the body of the rubber itself (again refer to Fig. 3.5 for a representative view of this construction).


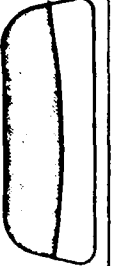




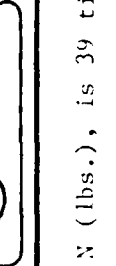
The swing pad design is a composite of several layers of rubber and brass material which has a concave bearing surface molded into it. This conformity serves two basic purposes. First of all, this pad puts more rubber into contact with the shaft it supports and, therefore, has the potential of operating with a lower unit pressure loading than the standard design. Secondly, the curvature and composition are such that loading will tend to form an entry wedge between the surface rubber and the rotating shaft. This entry wedge will facilitate the formation of a hydrodynamic water film at the bearing/shaft interface.

3.2 Description of Tests

A variety of laboratory test conditions were imposed upon each of the stave bearing sections shown previously in Fig. 3.5. These operating conditions are displayed in a tabularized matrix in Table 3-1. Over fifty independent friction versus speed curves were taken under the various loading and run-in conditions shown.

The run-in period for the test stave varied from a few minutes to several hours for the test runs. The test procedure attempted to evaluate the friction characteristics of the test staves in a "like new" condition, as well as in the "worn" condition. Two separate long term types of run-in were evaluated. In one of the tests the staves were merely operated for a long period of time (several hours) during which their performance was checked. In another set of tests the staves were put through an accelerated wear process and then retested for their change in friction behavior. This accelerated wear process involved removal of pad surface rubber with the aid of a fine (320 grit waterproof) emery paper. The removal of rubber was done by mating the test disk and pad while trapping the emery paper between the two. Sanding was performed under water and at the normal experimental load to be run after the process was complete. Each stave was "sanded" until the "worn" contact zone was equal in pattern width to that exhibited by stave sections which had been "run-in" without sanding.

TABLE 3-1
OPERATING TEST CONDITIONS

BEARING DESCRIPTION		SLIDING FRICTION CURVES FOR EACH • CONDITION NOTED											
		FRESH STAVE SECTION						ACCELERATED WEAR STAVE					
		Short Run-in*		Long Run-in*				Short Run-in*		Long Run-in*			
		Load Level		1		2		Load Level		1		Load Level	
	GROSS SECTION	1	2	3	4	5	6	1	2	3	4	5	6
SWING PAD		•											
BASIC STAVE		•	•	•	•	•	•	•	•	•	•	•	•
SMALL PIN (Centered)		•	•	•	•	•	•	•	•	•	•	•	•
MEDIUM PIN (Centered)		•	•	•	•	•	•	•	•	•	•	•	•
LARGE PIN (Centered)		•	•	•	•	•	•	•	•	•	•	•	•
LARGE PIN (Right Center)		•	•	•	•	•	•	•	•	•	•	•	•
LARGE PIN (Left Center)		•	•	•	•	•	•	•	•	•	•	•	•

* Normal load, N (lbs.), is 39 times (8.8 times) the load level number.

3.3 Results for Friction vs. Speed with Load Effects

Fig. 3.6 is a typical plot of test stave friction force measured as a function of sliding speed. The curve is representative of those gathered during testing. The low speed portion of the curve has a rapidly rising friction force which increases as sliding speed increases. At about 0.16 m/s (6.3 in/sec) and above the frictional force of the stave bearing drops off.

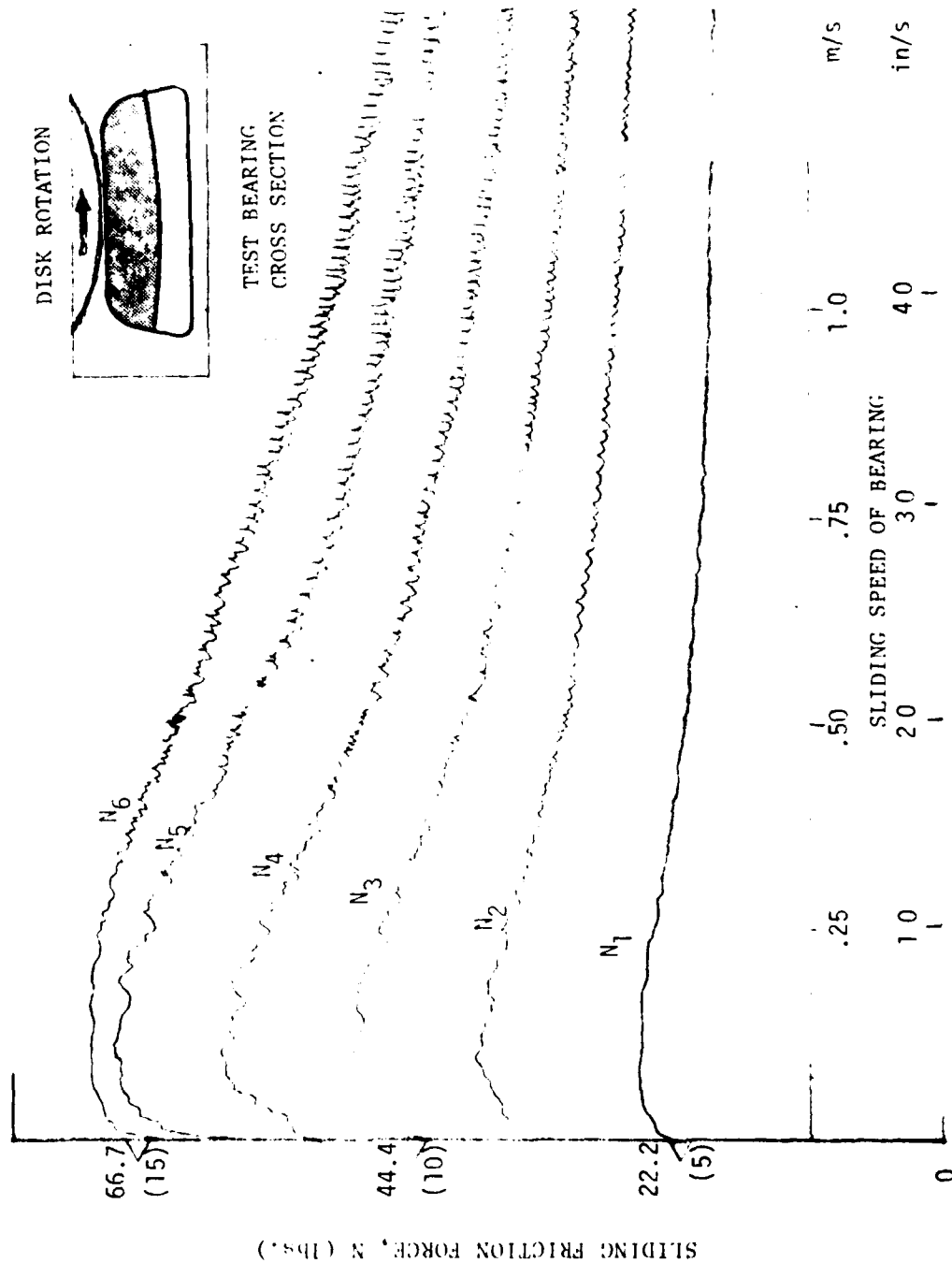
The friction versus speed plots taken during testing were quite smooth and repeatable; however, as seen in Fig. 3.6 small amplitude variations in frictional force are apparent. In particular, see the small spikes above 0.64 m/s (25 in/sec).

The source of these small oscillations was not identified positively during testing, but they were known to be in phase with the test disk rotation. These small variations in friction were thus attributed to disk run-out, normal loading changes, or to the local surface chemistry of the rotating disk.

In connection with the surface chemistry effect it was noted that a disk left in contact with the stave over a period of several days generated a much higher once-per-rev variation in sliding friction than one which had just been cleaned prior to testing. Thus, a standard disk surface cleaning operation was performed before each new stave element was tested.

Although qualitatively the character of the friction-speed plot of Fig. 3.6 is generally representative of all curves taken, the specific shape was found to depend upon

- The geometric design of the elastomeric bearing layer,
- The normal loading to which the bearing is subjected,
- The degree to which the pad has been worn-in,
- The ambient water temperature of operation, and
- The condition of chemical cleanliness of the shaft surface mated in sliding with the rubber bearing.



NORMAL LOADS	
Newton	(lbs.)
$N_1 = 1.98$	(8.8)
$N_2 = 3.97$	(17.6)
$N_3 = 5.96$	(26.5)
$N_4 = 7.95$	(35.3)
$N_5 = 9.93$	(44.1)
$N_6 = 11.9$	(53.07)

Figure 3.6 Friction-Speed Curves for Six Different Test Bearing Loads

The overall trends to some of these friction dependencies are shown in Fig. 3.7. Shown in that figure are six separate friction versus speed plots for each of six stave designs tested. Some of these show that friction drops continuously as the sliding speed increases. Most, however, reveal a low speed point at which the friction peaks out at a maximum for the test load applied.

Summary details of how sliding friction depends upon bearing load and bearing geometry are shown graphically in Fig. 3.8. In this figure are shown the six bearing stave cross-sections and their associated level of friction for the full range of test loadings. Each shaded curve gives the full envelope for all test speeds. Since 0.159 m/s (6.25 in/sec) represented the speed of maximum friction for these staves, the top of the shaded envelope represents a sliding speed of that value.

The friction-loading trends are evident from the various plots for each test stave shown in Fig. 3.8. Each stave geometry tested reveals a dependence of the coefficient of friction on loading level. A constant coefficient of friction would be represented by a straight line on this type of plot. It can be seen that in some of the test designs the friction coefficient increases as the load goes up, whereas, in some cases it decreases as the load is increased. In particular, the test stave with the large pin (centered) represents a case where the friction coefficient drops as loading is applied until a minimum friction level is reached; then the friction rises more rapidly with load than for most of the other designs.

In the test stave where the large pin is near the inlet of the bearing lubricant zone the friction level appears to rise continuously with loading. Under an increasing load situation it appears that this design has a tendency to inhibit the formation of a lubricating film more than any of the other designs tested. This tendency could account for the continuous rise with load observed in the friction force.

Table 3-2 indicates the degree to which the friction force magnitude changes as the bearing sliding speed increases. At a fixed normal load this difference in friction force change was taken from the friction traces at disk speeds of 0.079 m/s and 0.95 m/s. Consequently, Table 3-2 gives a

SUMMARY OF TEST FRICTION FORCES BY SPEED

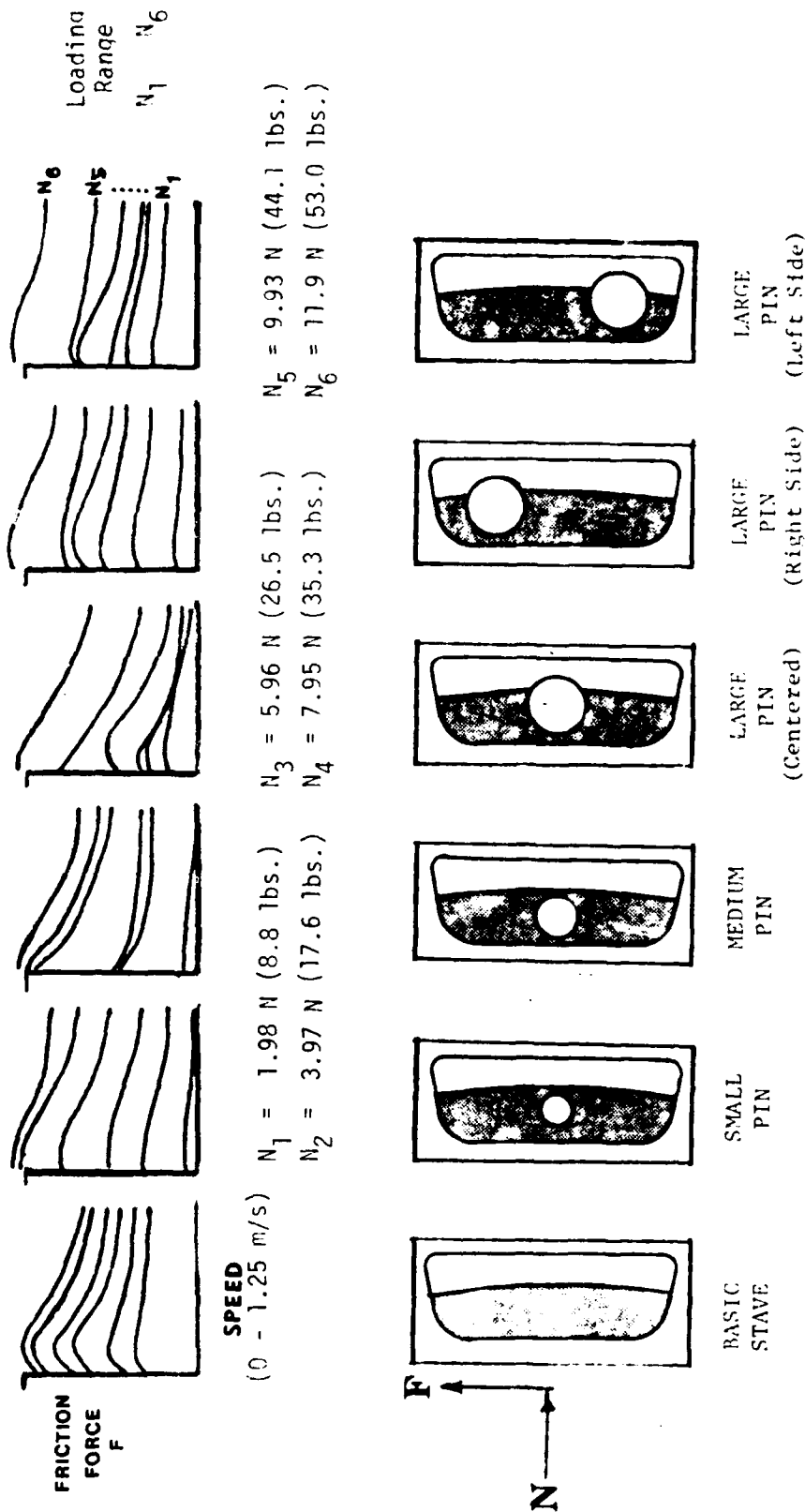
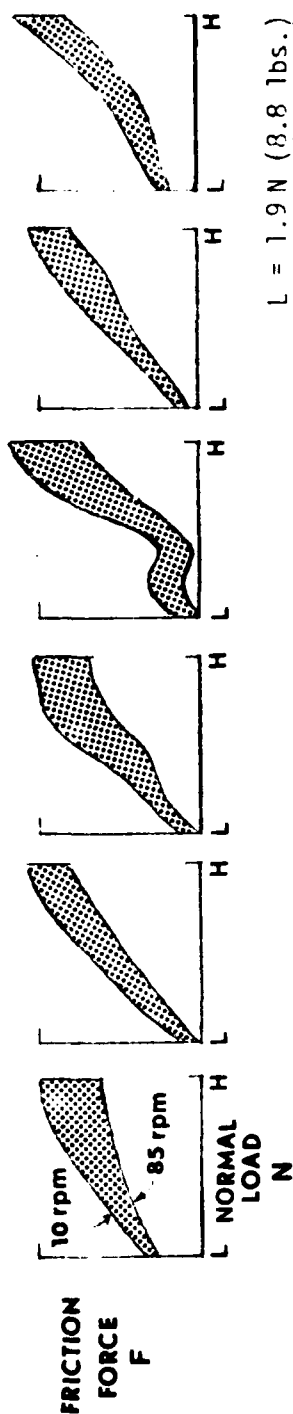


Figure 3.7 Friction Forces versus Sliding Speed for Full Range of Test Loads and Stave Design Cross Sections

SUMMARY OF TEST FRICTION FORCES BY LOADING

(10 rpm = .159 m/s 85 rpm = 1.36 m/s)



$L = 1.9 \text{ N}$ (8.8 lbs.)
 $H = 11.9 \text{ N}$ (53 lbs.)

TEST STAVE CROSS SECTIONS

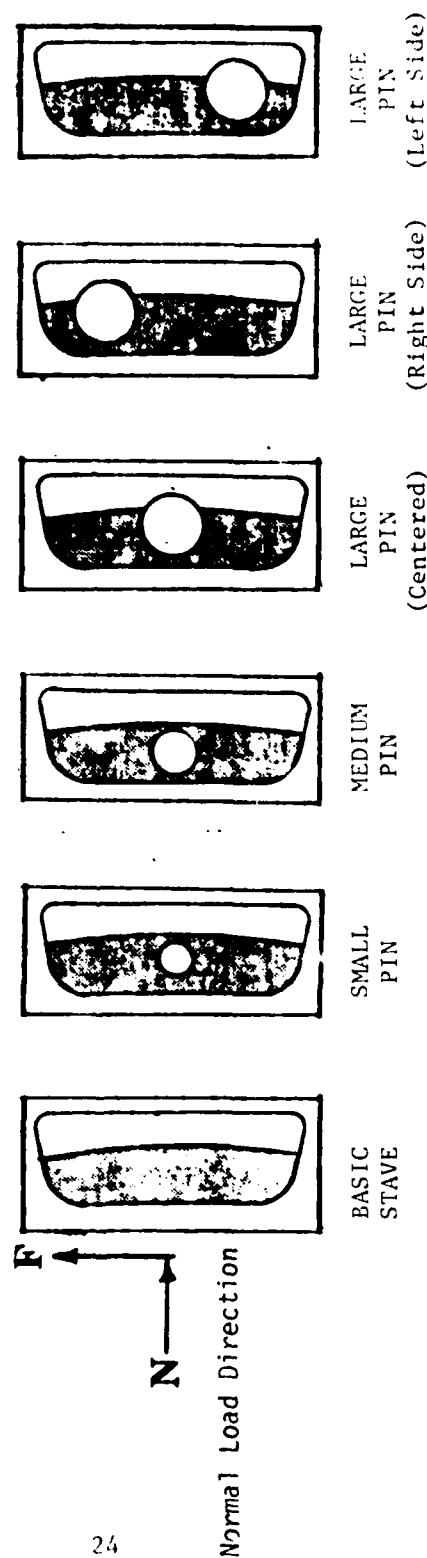


Figure 3.8 Friction Forces versus Normal Loading for Full Range of Test Speeds and Stave Design Cross Sections


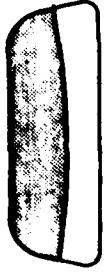





measure of the average negative slope of the friction-speed curve. (It is this slope which is the source of the squeal/chatter vibrations.) The table does not show the absolute level of friction force associated with the increase in sliding speed.

The values of frictional change shown in the table do not reveal a consistent trend when one compares the results between "short run-in" (less than five minutes) and "long run-in" (between six and eight hours). In some of the designs the chart shows a lowering of the friction difference as speed increases, whereas in most cases, it gets bigger. As indicated by the values in Table 3-2, the smallest change in friction force over the range of speed changes noted occurs in the stave design which has the large pin offset toward the trailing edge of the load zone. In this position the pin can act as a lubricating film converging mechanism since the stiffest portion of the pad is on the exit side of the sliding contact zone. This condition appears to reduce the change in friction force created by the stave as a result of increased sliding speed.

The largest change in friction occurs in the swing pad design after it has been provided with an accelerated wear profile. This is contrasted, however, with the fact that a "fresh" swing pad provided one of the lowest changes in friction with speed of any of the staves tested. In addition, the new swing pad exhibited, for most of the speed range, an extremely flat friction-speed relationship as compared to the other stave designs tested. The change in friction, however, is shown in Table 3-2 to be large since at low speeds the friction rises abruptly. The flat friction-speed nature of the new swing pad is shown in Fig. 3.9, and is contrasted with that for the "worn" pad which had been put through the accelerated wear process.

TABLE 3-2

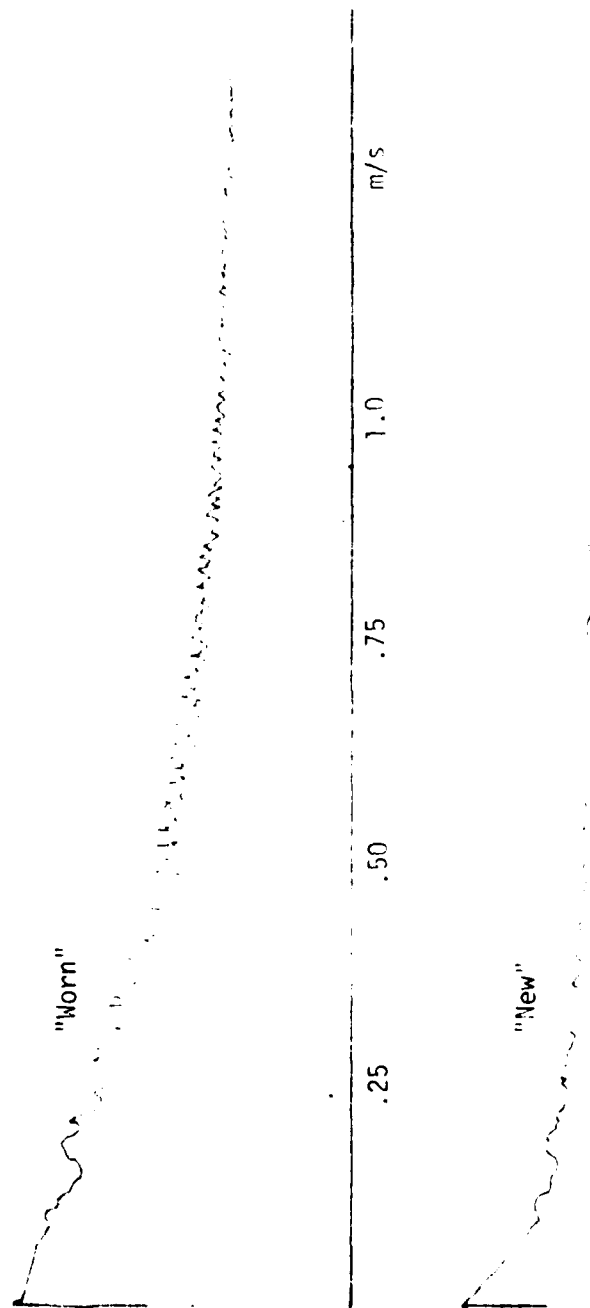
SLIDING FRICTION FORCE VARIATIONS

		DECREASE IN FRICTION FORCE MAGNITUDE (Newtons) WITH SPEED*					
		FRESH STAVE			WORN STAVE		
		Short Term Load Level 3	**	Long Term Load Level 3	Short Term Load Level 3	**	Long Term Load Level 3
	CROSS SECTION						
SWING PAD		17.8		13.3	33.4		37.8
BASIC STAVE		20.0		14.7	24.5		28.5
SMALL PIN (Centered)		15.6			26.7		24.5
MEDIUM PIN (Centered)		17.8		20.0	17.8		22.2
LARGE PIN (Centered)		16.5			20.0		22.2
LARGE PIN (Right Center)		8.9					
LARGE PIN (Left Center)		11.1			13.3		17.8

* Friction forces taken at 0.079 m/s and 0.95 m/s, respectively.

** Normal load N (lbs.) is 39 times (8.8) times the load level number.

SWING PAD TEST



SLIDING SURFACE FORCE

Figure 3.9 Swing Pad Friction Levels for Like "New" and "Worn" Stave Element that had been put through an Accelerated Wear Process

4.0 SUMMARY AND CONCLUSIONS

Laboratory tests were performed on a series of modified test staves in which the operational character of marine stern tube applications was simulated. Experiments were directed toward the frictional evaluation of stave design cross-sections which frequently operate in the boundary lubricated regime. The intent of the tests was to evaluate the extent to which the negative slope of the friction-speed curve could be modified by changes in stave design. The test rig used was similar to that discussed previously in Reference (4); however, the rig was modified for the present testing program.

Inspection of the test data revealed that:

- Stave bearing coefficients of friction were strongly influenced by pad loading and by the sliding speed of operation.
- Test stave frictional behavior was also determined to depend upon the cross-sectional design of the bearing pad.
- Stave friction level was found to depend upon the amount of "run-in" or extent of wear present on the stave surface.
- A comparison of the swing pad design to the other staves tested showed the swing pad to have three performance features that were different from those of the others tested:
 1. The friction of the swing pad always decreased as the sliding speed increased. Some of the other pad designs showed a peak friction near 0.16 m/s running speed.
 2. The friction-speed plot taken from a "new pad" was, in general, much flatter than that exhibited by other staves over the majority of the speed range tested.
 3. The friction level of a "new" swing pad drops to its minimum faster as sliding speed increases than does that of other designs tested. Since hydrodynamic wedge action is believed to be the reason for the friction to decrease with speed, the friction curve of the "new" swing pad suggests that a low

speed hydrodynamic wedge action is in evidence. In the "worn" condition, increased likelihood of intimate contact in the worn trough is probably the reason that the friction level remains close to the breakaway value.

Inspection of the data indicates that the shape of the friction-speed and friction-load curves are affected by the design of the stave. In particular, the thickness distribution of the elastomer across the stave does have a measurable influence on the slopes of these curves. Consequently, the data indicate that the design of the stave can have an effect on the tendency of the bearing to produce the unstable vibrations (caused by these negative slopes) which are commonly termed as "squeal" and "chatter."

5.0 RECOMMENDATIONS

The results of the work have indicated that the design of the stave affects the shapes of the friction-speed and friction-load curves, and thereby affects the tendency of the bearing to produce noise. Consequently, additional experimental work should be done in order to optimize (minimize) the low speed friction force dependence on speed and load. Of special importance is that this work be directed towards the swing pad, which has recently demonstrated promising performance in a sea trial.

The overall objective of the additional work should be to develop procedures for the design and construction of swing pad staves. This work should involve the experimental determination of how the differences in friction-speed behavior for conventional and swing pad staves arise. The work should also involve measurements of internal friction for these two stave types because the importance of internal damping on squeal/chatter is similar to that of the friction-speed curve. All measurements should be made not only for the conditions in the experimental apparatus, but also for more realistic stave length-to-width ratios and relative curvatures. Finally, the measurements should include not only that for friction force, but also those for water film thickness and rubber deformation at the inlet and outlet regions of the contact zone.

6.0 REFERENCES

1. Smith, W.V., and L.G. Schneider, "Lubrication in a Sea-Water Environment," Naval Engineers Journal, pp 841-854, October 1963.
2. Krauter, A.I., "Squeal of Water-Lubricated Elastomeric Bearings - An Exploratory Laboratory Examination," Shaker Research Corporation Report 77-TR-25, ONR Contract No. N00014-74-C-0278, December 1977.
3. Daugherty, T.L., and Sides, N.T., "Friction Characteristics of Water Lubricated Stave Bearings," David W. Taylor Naval Ship Research and Development Center, Report No. DTNSRC-80/023, February 1980.
4. Krauter, A.I., and Brower, D.C., "Squeal of Water-Lubricated Elastomeric Bearings - a Quantitative Laboratory Investigation," Shaker Research Corporation Report 78-TR-26, ONR Contract No. N00014-74-C-0278, November 1978.
5. Smith, R.L. et al, "Laboratory Examination of Vibration Induced by Friction of Water-Lubricated Compliant-Layer Bearings," Shaker Research Corporation Report 76-T12-18, ONR Contract No. N00014-74-C-0278, December 1976.
6. Smith, R.L., Pan, C.H.T., "An Exploratory Laboratory Simulation of Stick-Slip Induced Vibration of Water Lubricated Compliant Layer Bearings," Shaker Research Corporation Report 75-TR-11, ONR Contract No. N00014-74-C-0278, October 1975.

REPORT DISTRIBUTION

Defense Technical Information Center
Cameron Station
Alexandria, VA 22314 (12 copies)

Office of Naval Research
Code 438
800 N. Quincy Street
Arlington, VA 22217 (3 copies)

Mr. J. F. Dray Code 2832
David W. Taylor Naval Ship R & D Center
Annapolis, MD 21402 (2 copies)

Dr. Coda Pan
Shaker Research Corporation
Northway 10 Executive Park
Ballston Lake, NY 12019

Director
Office of Naval Research Eastern/Central Region
495 Summer Street
Boston, MA 02210

Library
Naval Academy
Annapolis, MD 21402

Richard W. Graham, II Code 5234
Naval Sea Systems Command
Sea 524, Room 375
Century Building, N.C.#4
Bearing and Seal Technology Branch
Washington, D. C. 20362 (5 copies)

Code 2627
Naval Research Laboratory
Washington, DC 20375 (2 copies)

Mr. Eli Arwas
Mechanical Technology, Inc.
968 Albany-Shaker Road
Latham, NY 12110 (2 copies)

Library
Naval Postgraduate School
Monterey, CA 93940

Prof. D. D. Fuller
Prof. H. G. Elrod
Department of Mechanical Engineering
Columbia University
New York, NY 10027

(Unpublished)

Friction and Lubrication Laboratory
The Franklin Institute Research Laboratories
The Benjamin Franklin Parkway
Philadelphia, PA 19103

Office of Naval Research
Code 473
800 N. Quincy Street
Arlington, VA 22207

